



1 **Impact of horizontal resolution and model time step on**
2 **European precipitation extremes in the OpenIFS 43r3**
3 **atmosphere model**

4
5 Yingxue Liu^{1,2}, Joakim Kjellsson^{1,2}, Abhishek Savita¹ and Wonsun Park^{3,4}

6
7 ¹GEOMAR Helmholtz Centre for Ocean Research Kiel, Kiel, Germany

8 ²Faculty of Mathematics and Natural Sciences, Christian Albrechts University of Kiel, Kiel, Germany

9 ³Center for Climate Physics, Institute for Basic Science (IBS), Busan, Republic of Korea

10 ⁴Department of Climate System, Pusan National University, Busan, Republic of Korea

11

12 *Correspondence to:* Yingxue Liu (yiliu@geomar.de)

13

14 **Abstract:** Events of extreme precipitation pose a hazard to many parts of Europe but are
15 typically not well represented in climate models. Here, we evaluate daily extreme precipitation
16 over Europe during 1982–2019 in observations (GPCC), reanalysis (ERA5) and a set of
17 atmosphere-only simulations at low- (100 km), medium- (50 km) and high- (25 km) horizontal
18 resolution with identical vertical resolutions using OpenIFS (version 43r3). We find that both
19 OpenIFS simulations and reanalysis underestimate the rates of extreme precipitation compared
20 to observations. The biases are largest for the lowest resolution (100 km) and decrease with
21 increasing horizontal resolution (50 and 25 km) simulations in all seasons. The sensitivity to
22 horizontal resolution is particularly high in mountain regions (such as the Alps, Scandinavia,
23 Iberian Peninsula), likely linked to the sensitivity of vertical velocity to the representation of
24 topography. The sensitivity of precipitation to model resolution increases dramatically with
25 increasing percentiles, with modest biases in the 70th–80th percentile range and large biases
26 above the 99th percentile range. We also find that precipitation above the 99th percentile mostly
27 consists of large-scale precipitation (~80 %) in winter, while in summer it is mostly large-scale
28 precipitation in Northern Europe (~70 %) and convective precipitation in Southern Europe
29 (~70 %). Compared to ERA5, the OpenIFS overestimates large-scale precipitation extremes in
30 winter, but underestimates in summer. The discrepancy between OpenIFS and ERA5 decreases
31 with increasing horizontal resolutions. We also examine the sensitivity of extreme precipitation
32 to model time step and find that the convective contribution to extreme precipitation is more
33 sensitive to the model time step than the horizontal resolution. This is likely due to the
34 sensitivity of convective activity to model time step. On the other hand, the large-scale
35 contribution to extreme precipitation is more sensitive to horizontal resolution than the model



36 time step, which may be due to sharper fronts and steeper topography at higher horizontal
37 resolution.

38

39 **1. Introduction**

40

41 Extreme precipitation events have severe impacts on human society and ecosystems. For
42 example, Germany experienced extreme precipitation during mid-July 2021, which exceeded
43 100 mm/d over a large area resulting in a devastating flood. The recent flood is one of the most
44 serious natural disasters for Germany since 1962, in which around 180 people died as a result
45 of the flood. Coupled Model Intercomparison Project (CMIP) models are used to understand
46 the present and future climate. The CMIP5 models project that the frequency of the most
47 intense precipitation observed today in Europe would be almost double in the future at each
48 1°C of warming (Myhre et al., 2019). Recently the CMIP6 models also projected an increase
49 in extreme precipitation over most of the regions under global warming (Intergovernmental
50 Panel on Climate Change, 2023; Li et al., 2021). The increasing extreme precipitation poses a
51 threat for society and must thus be realistically simulated and projected accurately for future
52 climates. However, the climate models have large uncertainties in simulating extreme
53 precipitation events due to lack of observations, coarse horizontal resolution grid, long model
54 time step etc. (Alexander et al., 2019; Avila et al., 2015; Sillmann et al., 2013). This study aims
55 to understand the sensitivity of extreme precipitation to model resolution and time step.

56 The CMIP models can simulate time-mean precipitation very well but usually underestimate
57 the intensity and frequency of extreme precipitation (O’Gorman, 2015; Sillmann et al., 2013).

58 The intensity of simulated extreme precipitation often increases with increased horizontal
59 resolution in atmosphere models (Caldwell, 2010; Rauscher et al., 2016; Wehner et al., 2010,
60 2014). Jong et al. (2023) analyzed the extreme precipitation in Northeastern United States (US)
61 using the Seamless system for Prediction and EArth system Research (SPEAR) and Large
62 Ensemble of Community Earth System Model version 1 (CESM-LE) model simulations at
63 different horizontal resolutions, and they found that a model with 25 km horizontal resolution
64 simulates much more realistic frequency, amplitude, temporal variability and trends in extreme
65 precipitation than 50 and 100 km model resolution. However, Kopparla et al. (2013) found that
66 the reduced biases at higher horizontal resolution do not hold for all regions. They concluded
67 that extreme precipitation with finer model resolutions in Community Atmospheric Model



68 version 4 (CAM4) has better agreement with observational datasets in Europe and the US, but
69 not in Australia.

70 Considering the time and computational cost, climate simulations of more than 100 years are
71 generally not feasible with high-resolution (25 km or higher) models. Instead, regional climate
72 models (RCMs) are developed by focusing on a particular region, where higher-resolution
73 model simulations can be conducted with reduced cost (Laprise, 2008). Strandberg & Lind
74 (2021) compared the precipitation using both global (CMIP5, CMIP6 and HighResMIP) and
75 regional (CORDEX RCMs) model simulations at different resolutions (~300–12.5 km) and
76 found that high-resolution models reduce the biases for extreme precipitation. They also found
77 that the effect of horizontal resolutions for extreme precipitation is mostly in regions with
78 complex topography and in the summer season when precipitation is mostly caused by
79 convective processes, in agreement with Iles et al. (2020). The reduced biases in extreme
80 precipitation near topography in high-resolution models is mostly due to an improved
81 representation of topography, coastlines, and small-scale processes such as convection and
82 diffusion. However, Strandberg & Lind (2021) showed that models with higher horizontal
83 resolution overestimate the intensity of extreme precipitation in some regions over Europe.
84 Moreover, once reaching 50 km, the improvement is smaller for further higher resolution,
85 which is consistent with Demory et al. (2020), as they found the effect of increasing resolution
86 from 50 to 12 km grid on the daily precipitation distributions is smaller outside the mountainous
87 and coastal regions. However, Chan et al. (2013) investigated the precipitation in regional
88 models with 50, 12 and 1.5 km grid spacing over the southern UK and found that the
89 representation of daily orographic precipitation improved when increasing horizontal
90 resolution from 50 km to 12 km, but not from 12 km to 1.5 km. Chan et al. (2013) found that
91 1.5 km simulations (convection-permitting) predominantly improve the representation of
92 extreme precipitation on sub-daily timescales but not for daily timescales, which is further
93 consistent with Prein et al. (2013). The small improvements for extreme precipitation in higher
94 horizontal resolution simulations indicate that although the bias of daily extreme precipitation
95 is reduced with finer horizontal resolution, there is also a “diminishing return”.

96 No global atmosphere-model simulations in the Atmosphere Model Intercomparison Project
97 (AMIP) in CMIP6 explicitly resolve convection and all must therefore employ
98 parametrizations of such motions and users must carefully choose the associated parameters.
99 The cloud microphysics is sensitive to the model time step in an idealized convection-



100 permitting model, e.g., the precipitation is reduced 53 % when the time step was lengthened
101 from 1s to 15 s (Barrett et al., 2019). Mishra & Sahany (2011) also found a more realistic
102 simulation of the precipitation pattern in the tropics when the time step was shortened from 60
103 min to 5 min. Wan et al. (2021) found that 10-year mean zonal averages change when the time
104 step is reduced by a factor of 6, such as the temperature, cloud fraction, and the relative
105 humidity in the troposphere. Bador et al. (2020) showed that models at higher horizontal
106 versions (50 km or 25 km) where convection parameters were not re-tuned to the increased
107 resolution often exhibit larger biases than corresponding model versions at lower horizontal
108 resolution.

109 A recent study by Savita et al. (2024) explored the sensitivity of global mean precipitation to
110 the horizontal resolution and model time step in atmosphere-only simulations with OpenIFS.
111 However, the extreme precipitation sensitivity to horizontal resolution and time step was not
112 investigated. In this study, we investigate the impact of horizontal resolutions (~100 km, ~50
113 km, and ~25 km) and model time steps (60 minutes, 30 minutes, and 15 minutes) on daily
114 extreme precipitation using OpenIFS simulations and compare them with observation. This
115 paper is structured as follows: section 2 describes the data and methodology, and section 3
116 discusses the results. The conclusion and discussion can be found in section 4.

117

118 **2. Data and Methods**

119

120 **2.1 Model, observation, and reanalysis data**

121

122 The OpenIFS is derived from the Integrated Forecasting System at the European Centre for
123 Medium-range Weather Forecasting (ECMWF-IFS) cycle 43 release 3 (43r3) (ECMWF, 2017).
124 We use the same AMIP simulations that were used in Savita et al. (2024) which cover the
125 period 1979-2014 and are extended to 2019 using sea-surface temperature (SST) from ERA5
126 and the Shared Socioeconomic Pathway 5 (SSP5-8.5) scenario from CMIP6. OpenIFS
127 simulations use 91 vertical levels (L91) and the different horizontal resolutions: low resolution
128 (Tco95, ~100 km), medium resolution (Tco199, ~50 km), and high resolution (Tco399, ~25
129 km). For the low resolution, additional sensitivity experiments use different model time steps
130 i.e., 60, 30, and 15 minutes and we refer to these experiments as LR60m, LR30m, and LR,
131 respectively. For medium and high resolution, the same model time step is used (i.e., 15
132 minutes), of which experiments refer to as MR and HR, respectively. While the OpenIFS uses



133 a reduced octahedral grid (Malardel et al., 2016), the final output used in this study has been
134 interpolated to a regular grid using the XIOS output server. The LR, LR30m and LR60m data
135 were interpolated to a global 0.9° grid while the MR and HR data were interpolated to a global
136 0.45° grid, i.e., we are not investigating extreme precipitation in high resolution simulations in
137 their native grid, which will be investigated in future study. The simulations used here were
138 used by Savita et al. (2024) who found improvements in the surface zonal wind, Rossby wave
139 amplitude and phase speed, weather regime patterns, and surface-air temperature when
140 reducing a model time step from 60 minutes to 30 and 15 minutes in low resolution or
141 increasing the horizontal resolution from 100 km to 50 and 25 km. However, Savita et al. (2024)
142 did not find such improvement in the mean precipitation bias by increasing horizontal
143 resolution or reducing the model time step.

144 To validate OpenIFS simulations, we use the gridded daily precipitation observational data
145 from Global Precipitation Climatology Centre (GPCP) with resolution of $1^\circ \times 1^\circ$ for the period
146 1982–2019 (Ziese et al., 2022) as well as the reanalysis data from the ECMWF Reanalysis v5
147 (ERA5) for 1979–2019 (Hersbach et al., 2023). ERA5 is based on the IFS Cy41r2, with 31 km
148 horizontal resolution and 137 levels (Hersbach et al., 2020). We analyzed total, large-scale,
149 and convective precipitation in this study. The total precipitation (convective plus large-scale
150 precipitation) in the IFS is the accumulated precipitation, comprising of rain and snow, that
151 falls to the Earth’s surface, and it is not assimilated in the IFS. The convective precipitation is
152 generated by the convection scheme in the IFS, which represents convection at spatial scales
153 smaller than the grid box. The convection scheme follows Sundqvist (1978), which is also used
154 in the OpenIFS. The large-scale precipitation is generated by the cloud scheme (Khairoutdinov
155 & Kogan, 2000), which represents the formation and dissipation of clouds and large-scale
156 precipitation due to changes in atmospheric quantities (such as pressure, temperature, and
157 moisture) predicted directly by the IFS at spatial scales of the grid box or larger. The
158 autoconversion/accretion parameterization is a non-linear function of the mass of both liquid
159 cloud and rainwater. The calculation follows Khairoutdinov & Kogan (2000) which is derived
160 from large eddy simulation studies of drizzling stratocumulus clouds, and this scheme is also
161 used in OpenIFS. Several studies have evaluated the performance of ERA5 and found that the
162 total precipitation in ERA5 is performing well over the US (Tarek et al., 2020; Xu et al., 2019).
163 For global precipitation, the mean absolute difference over 50° S–50° N between ERA5 and
164 TRMM/3B43 is 0.58 mm/d; the global-mean correlation with GPCP data is 0.77, which is



165 better compared to ERA-Interim (0.63 mm/d and 0.67) (Hersbach et al., 2020). ERA5 also
166 performs well in polar regions in representing wind, temperature and humidity (Graham et al.,
167 2019; Tetzner et al., 2019; Wang et al., 2019).

168 Here we analyze daily ERA5 and the OpenIFS data over Europe (30° N–72° N, 10° W–40° E)
169 for the period of 1982–2019 to be consistent with GPCP dataset. For comparison, the ERA5,
170 GPCP, MR, and HR data are remapped to LR (~0.9375° × 0.9375°) using the second-order
171 conservative remapping method. The second-order conservative method includes the gradient
172 across the source cell, which is not included in the first-order conservative method. Therefore,
173 it gives a smoother, more accurate representation of the source field (Jones, 1998).

174

175 **2.2 Methods**

176 **Calculation of q^{th} percentile value**

177 We calculated different percentile values using total precipitation from GPCP, ERA5, and
178 OpenIFS simulations. When we calculated the q^{th} percentile value, the normalized ranking
179 usually did not match the location of the q^{th} percentile exactly, which means the q^{th} lies between
180 two indices. Therefore, we determined the location first, then computed the q^{th} value by
181 interpolating between the two nearest values based on the location. Here we used the formula
182 below to find the location:

$$183 \quad j = q \cdot (n-1) \quad (1)$$

184 n is the length of the sample, q is the desired percentile, j is the location which is the distance
185 from the first value X_1 (X_m are the sorted sample values, $m=1, 2, \dots, n$). Then we took i as the
186 nearest (lower) integer of j to get the q^{th} value $P(q)$ by interpolating.

$$187 \quad P(q) = X_i + (X_{i+1} - X_i) \cdot (j-i) \quad (2)$$

188 There are other methods to determine the location of q^{th} percentile (Hyndman & Fan, 1996),
189 but here we use the ‘linear’ one.

190

191 **The convective contribution to extreme precipitation**

192 To calculate the contribution of convective precipitation to total precipitation for a percentile
193 range, at each grid point we accumulated the convective precipitation on all days when the total
194 precipitation is in that percentile range, then divided it by the accumulated total precipitation
195 on those days to get the fraction of convective precipitation.

196

197



198 Calculation of RMSE values

199 We used the root-mean-square error (RMSE) referenced to GPCC that measures the
200 performance of ERA5 and OpenIFS simulations:

$$201 \quad \text{RMSE} = \sqrt{\frac{\sum_{i=1}^n (x_{mi} - x_{oi})^2}{n}} \quad (3)$$

202 x_{mi} is the value at i grid point for ERA5 or OpenIFS simulations, x_{oi} is the value for GPCC, n
203 is the number of land grid points over Europe. Using equation (3), we calculated the RMSE
204 values for different percentile ranges. Smaller RMSE values mean the biases between OpenIFS
205 (or ERA5) and GPCC are smaller i.e., the model simulations and ERA5 are performing better.

206

207 Confidence intervals

208 We calculated the 2.5 to 97.5th confidence intervals (CI) for the RMSE for each percentile with
209 a bootstrap method. For example, to calculate the CI for the RMSE of HR (referenced to GPCC
210 observation), we randomly chose n grid cell pairs from GPCC and HR over European land,
211 then calculated their RMSE (n is the number of total land grid points over Europe). This process
212 was repeated for 2000 times. We took the 2.5th and 97.5th percentiles of the distribution of the
213 2000 RMSEs as the 95 % CI. If the CI for different simulations do not overlap then we refer
214 that they are significantly different.

215

216 3. Results

217

218 3.1 Extreme precipitation over Europe

219

220 We show the time series of 99th percentile precipitation calculated from all grid points and all
221 days in each year over the period 1982–2019 from GPCC, ERA5, and OpenIFS simulations
222 over Europe (Fig. 1). The ERA5 simulates an inter-annual variability of the 99th percentile
223 precipitation similar to that in GPCC. For example, the peak in 2010 and the low in 1994 are
224 well reproduced in the ERA5. OpenIFS simulations do not reproduce the same inter-annual
225 variability as in GPCC or ERA5 but LR and HR do reproduce the 95 % significant positive
226 trend observed in GPCC (0.03 mm/d/y, not shown), which are ~0.2 mm/d/y for both LR and
227 HR, and it is not significant for MR. We note that the OpenIFS simulations use observed SST
228 and sea-ice concentrations as boundary conditions, but ozone is taken from a photochemical
229 equilibrium (Cariolle & Teyssède, 2007) and aerosol concentrations are taken from
230 Copernicus Atmosphere Monitoring Service (CAMS) monthly climatology. Therefore, we do
231 not expect LR, MR and HR to reproduce trends driven by ozone or aerosols forcing. We also



232 find that both ERA5 and OpenIFS simulations have relatively lower 99th percentile
233 precipitation rates compared to GPCC (Fig. 1). The RMSE for ERA5 (0.36 mm/d) is lower
234 than for OpenIFS simulations which is largest for LR (2.03 mm/d) and decreases with
235 increasing horizontal resolution (i.e., 1.13 mm/d for MR and 0.69 mm/d for HR). Note that Fig.
236 1 does not contain any spatial information and that a mismatch between model data and
237 observations can be due to the 99th percentile occurring in different regions and/or with
238 different magnitudes. The RMSE analysis suggests that ERA5 and HR are close to GPCC and
239 LR is far from GPCC.

240

241 Figure 2a–e shows the spatial distribution of the 99th percentile precipitation over Europe for
242 all days in each season for all years in GPCC, ERA5, and OpenIFS simulations, respectively.
243 In general, the extreme precipitation is very low (~2 mm/d) in Northern Africa, which is to be
244 expected since the mean precipitation is only 0.5 mm/d in those regions (Fig. S1). The extreme
245 precipitation exceeds 30 mm/d over mountain areas (e.g., Scandinavian mountains, Alps, and
246 Iberian Peninsula) and the north coast of the Mediterranean but is otherwise lower (~15 mm/d).
247 The spatial distribution of extreme precipitation matches that of the mean precipitation pattern
248 (Fig. S1). The high 99th percentile precipitation near mountains is likely due to the forced ascent
249 of westerly (Scandinavia, Iberian Peninsula, British Isles) and southerly (Alps) winds. The high
250 99th precipitation in the north of the Mediterranean is likely because of warm and moist
251 southerly winds from the Mediterranean Sea. The ERA5 and OpenIFS simulations overall
252 reproduce the spatial distribution of the 99th percentile precipitation from GPCC. However, the
253 magnitudes are different, particularly over the Scandinavian mountains, the Alps, and central
254 Europe near 50° N (Fig. 2a–e). Figure 2f–i show the regional biases for the 99th percentile
255 precipitation referenced to GPCC. LR mostly underestimates the 99th percentile precipitation
256 in mountainous areas and deserts by more than 25 % (Fig. 2g) and the biases are reduced when
257 horizontal resolution is increased in MR and HR (Fig. 2h–i). We also notice that LR
258 underestimates the 99th percentile precipitation south of the Alps but overestimates it to the
259 north (Fig. 2 (g)), whereas this bias is negligible in higher-resolution simulations (Fig. 2h–i).
260 Lavers et al. (2022) also found too much extreme precipitation on the north side of the Alps in
261 ERA5 during a storm. This could be because the moist southerly winds do not ascend high
262 enough with LR, therefore there is less precipitation formed on the southern side and more
263 moisture is advected over the mountain. The reduced biases near mountain regions in the
264 higher-resolution simulations are likely because higher resolution has a better representation



265 of topography and vertical velocity. A cross section of the topography and annual-mean vertical
266 velocity at 850 hPa and 62° N (Fig. S2 and S3) highlight that the higher-resolution simulations
267 resolve steeper topography, which leads to more ascent and thus more precipitation.

268

269 The 99th percentile precipitation over the Alps is more realistic with higher horizontal
270 resolution compared to lower resolution. However, all simulations as well as ERA5 exhibit a
271 negative bias over northeast Italy and west Slovenia (Fig. 2f-i). The cause could be a bias in
272 GPCC or a persistent model bias in the ECMWF-IFS on which both ERA5 and OpenIFS are
273 based. In general, ERA5 has a lower RMSE (2.6 mm/d) for extreme total precipitation than
274 OpenIFS simulations, i.e., ERA5 has overall lower biases than LR (4.0 mm/d) and is similar to
275 MR (3.0 mm/d) and HR (2.9 mm/d).

276

277 We next calculate the trend for the annual 99th percentile precipitation over Europe (Fig. S4 &
278 S5) and find that the 99th percentile precipitation has a large positive trend in central Europe
279 and a negative trend to the north of the Alps in GPCC (Fig. S4a). The ERA5 reproduces the
280 pattern of the trend found in GPCC but not significant. However, OpenIFS simulations do not
281 have consistent patterns with GPCC (Fig. S4c-e, Fig. S5c-e), with only LR60m reproducing
282 the large positive trend in central Europe (Fig. S5c). Overall, the trend is largely underestimated
283 over central Europe but overestimated over northern Europe in OpenIFS simulations. We have
284 not found any consistent improvement across the horizontal resolution and model time step.

285

286 In addition to the 99th percentile precipitation, we calculate annual total precipitation in
287 different percentile ranges, such as 70th-80th, 80th-90th, 90th-95th, 95th-99th, 99th-99.5th, 99.5th-
288 99.9th and larger than 99.9th (i.e., >99.9th) percentile. We calculate the RMSEs for ERA5 and
289 OpenIFS simulations referenced to GPCC in each range and find that the RMSEs for ERA5
290 and OpenIFS simulations vary strongly across percentile ranges (Fig. 3). The RMSEs increase
291 exponentially with increasing percentiles, from less than 1 mm/d at the 70th-80th percentile
292 range to ~8 mm/d above the 99.9th percentile range. The largest RMSE is found for LR60m
293 above the 99.9th percentile range which is around 12 mm/d [CI: 11.3-12.8 mm/d]. We also find
294 that the RMSEs decrease with finer horizontal resolution for all percentile ranges. The CI of
295 the RMSEs from LR do not overlap with those from higher horizontal resolutions for any
296 percentile range, i.e., the biases from LR are significantly different from that at higher
297 resolutions and thus clearly sensitive to the horizontal resolution. We also find that the RMSE



298 differences between LR simulation and the higher-resolution simulations as well as ERA5 are
299 larger at higher percentile ranges ($>95^{\text{th}}$) than those at lower percentile ranges ($<95^{\text{th}}$). Thus,
300 we conclude that extreme precipitation is more sensitive to horizontal resolution than
301 precipitation at lower percentile ranges ($<95^{\text{th}}$). ERA5 has the smallest RMSE of all datasets
302 above the 95^{th} percentile ranges, i.e., ERA5 has a better representation of the extreme
303 precipitation than our OpenIFS simulations (Fig 3).

304

305 The RMSEs for LR60m, LR30m, and LR are increasing with increasing model time steps.
306 However, the CI of RMSE overlap at all percentile ranges, i.e., the sensitivity of precipitation
307 to the model time step is not statistically significant in the low-resolution configurations. While
308 the model time step may influence precipitation, especially convective precipitation, errors
309 from poorly resolved topography probably have a large impact on the RMSE, which would
310 explain the lack of sensitivity to the model time step.

311

312 **3.2 Relative roles of convective and large-scale precipitation**

313

314 We calculate the fractions of convective and large-scale precipitation in total precipitation for
315 days when the total precipitation exceeds the 99^{th} percentile in all model simulations and ERA5
316 (Fig. 4 & 5). Note that, GPCC does not provide convective and large-scale precipitation
317 separately, therefore we compare our OpenIFS simulations to the ERA5 dataset to assess the
318 realism of the model simulations. We note that ERA5 is a reanalysis dataset where precipitation
319 is a parametrized variable, and observations of which are not assimilated over Europe. ERA5
320 monthly precipitation has a good agreement with GPCC on the land, with correlations above
321 90 % for most of Europe, and above 70 % for Australia, Asia, and North America (Bell et al.,
322 2021). ERA5 also shows smaller biases for mean precipitation than other reanalysis datasets in
323 the tropics compared to the Global Precipitation Climatology Project (GPCP), with relative
324 biases of 13 % for ERA5, 17 % for MERRA-2 and 36 % for JRA-55 (Hassler & Lauer, 2021).
325 The biases for mean precipitation are found smaller over extra-tropics than the tropics
326 compared to the gauge-based precipitation observations, particularly agreeing well with
327 observations over central Europe and South Asia (Lavers et al., 2022). Moreover, ERA5 can
328 capture the locations and patterns of highest precipitations in observations, but cannot simulate
329 the magnitude (Lavers et al., 2022). We also find that the extreme precipitation over Europe in
330 ERA5 is closer to observations than models (Fig. 1, 2, and 3), therefore, we use ERA5 for the
331 benching mark here although it has some known biases.



332

333 The ERA5 data and OpenIFS simulations show that, in DJF, the extreme precipitation is nearly
334 100 % large-scale precipitation over northern Europe, more than 90 % over central Europe,
335 and more than 70 % over western and southern Europe (Fig. 5a–d). However, in JJA, large-
336 scale precipitation makes up most of the extreme precipitation over northern Europe (>70 %)
337 while convective precipitation makes up most of the extreme precipitation in the Mediterranean
338 region (>70 %) (Fig. 4a–d). The OpenIFS simulations largely reproduce the pattern of the
339 fraction of convective precipitation found in ERA5, but we note differences in magnitudes (Fig.
340 4e–g, and Fig. 5e–g)). In JJA, the OpenIFS simulates the contribution of the convective
341 precipitation quite well over Scandinavia where the extreme precipitation is mostly large-scale
342 precipitation, but overestimates that for other areas over Europe (Fig. 4e–g). The RMSEs from
343 MR (0.10 mm/d [CI: 0.09–0.10 mm/d]) and HR (~0.09 mm/d [CI: 0.09–0.10 mm/d]) are not
344 significantly different, while LR (~0.12 mm/d [CI: 0.12–0.13 mm/d]) is significantly larger
345 than those in MR and HR. In DJF, the OpenIFS underestimates the contribution from
346 convective precipitation except for near-coastal areas (Fig. 5e–f). That is, the contribution from
347 large-scale precipitation is overestimated, and the bias is reduced with higher horizontal
348 resolution, i.e., in MR and HR.

349

350 Further, we explore the relative roles of horizontal resolution and time step for the large-scale
351 and convective precipitation at different percentile ranges (Fig. 6). In general, the RMSEs
352 increase with increasing percentiles, but also decrease with increasing horizontal resolution and
353 shorter model time step. The RMSE reduces for higher percentile in higher resolution due to
354 better representation of topography, and in smaller model time step due to enhanced convection.
355 The exceptions are the total precipitation above the 99.5th percentile in JJA where the RMSEs
356 from LR are larger than LR30m (Fig. 6a), and the convective precipitation above the 99th
357 percentile in JJA and DJF where the RMSEs from HR are larger than MR (Fig. 6c & f).

358

359 The CI for RMSEs of total precipitation from LR, MR and HR in DJF and JJA do not overlap
360 for all percentile ranges, thus there is a significant sensitivity of the total precipitation to the
361 horizontal resolution, particularly for extreme total precipitation. The exceptions are the total
362 precipitation below the 90th percentile ranges and above the 99.9th percentile range in JJA
363 where the CI for RMSEs in MR and HR overlap (Fig. 6a). However, the sensitivity is not found
364 for the global-mean total precipitation by increasing horizontal resolution (Savita et al., 2024).



365 For the large-scale precipitation in JJA, the CI for RMSEs from LR do not overlap with those
366 from MR and HR at higher percentile ranges ($>95^{\text{th}}$), but overlap at lower percentile ranges
367 ($<95^{\text{th}}$) (Fig. 6b). That is, the large-scale precipitation from the extreme precipitation is
368 sensitive to the horizontal resolution. We note that a reduced bias is not found for the
369 convective precipitation in JJA (Fig. 6c), and we conclude that the horizontal resolution
370 dependence of extreme total precipitation in JJA comes from the large-scale precipitation. For
371 DJF, the large-scale precipitation is sensitive to the horizontal resolution for all percentile
372 ranges, where the CI for RMSEs in LR do not overlap with those from MR and HR (Fig. 6e).
373 The convective precipitation in DJF is also sensitive to the horizontal resolution (Fig. 6f),
374 however there is little convection precipitation in DJF, thus the sensitivity for convective
375 precipitation in DJF is not important. Therefore, the resolution dependence of extreme total
376 precipitation is mostly dominated by the large-scale precipitation in DJF.

377

378 For the model time step, the CI for RMSEs of total precipitation from LR60m, LR30m, and
379 LR overlap at all percentile ranges in both JJA and DJF (Fig. 6a & d), i.e., the extreme total
380 precipitation is not sensitive to the model time step in a significant way in the low-resolution
381 simulations. Similarly, the mean total precipitation is also found insensitive to the model time
382 step (Savita et al., 2024). Both the large-scale and convective precipitation are sensitive to the
383 model time step particularly above the 95^{th} percentile ranges in JJA (Fig. 6b & c). The
384 convective precipitation is more sensitive to the model time step than the large-scale
385 precipitation in JJA, but in DJF the sensitivity is found only for the large-scale precipitation
386 (Fig. 6e). Also, the lack of sensitivity for convective precipitation in DJF may be because there
387 is almost no convective precipitation in DJF.

388

389 **4. Discussion and Conclusion**

390 We have investigated the sensitivity of extreme precipitation across different horizontal
391 resolutions and model time steps in atmosphere-only experiments with the OpenIFS.
392 Comparing extreme precipitation (defined as total daily precipitation at the 99^{th} percentile)
393 from OpenIFS simulations, reanalysis (ERA5), and observation (GPCC), we find that MR and
394 HR mostly better represent the precipitation extremes compared to LR. We also found a more
395 significant sensitivity to the horizontal resolution for the precipitation above the 95^{th} percentile
396 and less sensitivity for lower percentile ranges ($<95^{\text{th}}$) (Fig. 3). These OpenIFS-based results
397 are similar to Kopparla et al. (2013), who found that the bias of extreme precipitation in the
398 high-resolution simulation (25 km) is reduced compared to the lower-resolution simulations



399 (100 km and 200 km) over Europe in their atmospheric model, but not for precipitation at lower
400 percentiles (i.e., <95th). However, the sensitivity to the horizontal resolution found by Kopparla
401 et al. (2013) was not significant over Europe which is rather different from our results as we
402 have found a significant difference across the horizontal resolutions. In contrast to the extreme
403 precipitation, the bias for global mean precipitation is not decreasing when increasing
404 horizontal resolution from ~200 km to ~100 km or ~50 km in the ECHAM6-AMIP simulations
405 (Hertwig et al., 2015), and also in other GCMs (e.g., OpenIFS, HadGEM1 and HadGEM3)
406 (Demory et al., 2020; Savita et al., 2024; Schiemann et al., 2014). However, Delworth et al.
407 (2012) found an improvement in the global mean precipitation with increasing horizontal
408 resolution in a coupled model (GFDL).

409

410 The improvements due to increasing horizontal resolution for the extreme precipitation are
411 mostly over the mountain areas, consistent with previous studies which found the effect of
412 horizontal resolution being largest in areas with complex topography over Europe and also
413 other regions for mean and extreme precipitation (Demory et al., 2020; Iles et al., 2020;
414 Monerie et al., 2020; Prein et al., 2013; Torma et al., 2015). The sensitivity to the horizontal
415 resolution comes from the large-scale precipitation, which is likely because of the better-
416 resolved topography. However, the convective precipitation in JJA is more sensitive to the
417 model time step than it is to the horizontal resolution, likely because there is an increase in
418 shallow and mid-level convection with a shorter time step in the OpenIFS (Savita et al., 2024),
419 thus we get more convective precipitation.

420

421 In our results, larger improvements are obtained when the horizontal resolution is increased
422 from LR to MR, but relatively smaller improvements from MR to HR. Similar results are also
423 found in Roberts et al. (2018), where the climatological surface biases are relatively insensitive
424 when increasing the atmospheric resolution from ~50 km to ~25 km in the ECMWF-IFS. Jung
425 et al. (2012) also showed that the largest improvements in extratropical cyclones, Euro-Atlantic
426 blocking, tropical mean precipitation, and tropospheric circulation are found when increasing
427 horizontal resolution from 126 km to 39 km with relatively small further changes from 39 km
428 to 16 and to 10 km in ECMWF atmosphere model. Kopparla et al. (2013) and Bacmeister et al.
429 (2014) found much improvement for the mean precipitation and extreme precipitation with the
430 increasing atmospheric resolution from ~200 km to 100 km, but less improvement from ~100
431 km to ~25 km. It is likely due to a lack of tuning with the changing horizontal resolution. The
432 above conclusions are valid over Europe, but also valid for other regions such as the tropics



433 and subtropics. For example, the predictions of tropical cyclone intensity are markedly
434 improved when the horizontal resolution of the atmosphere model is increased from 120 km to
435 40 km, but not for 15 to 10 km (Jung et al., 2012), which often triggers extreme precipitation
436 (Gori et al., 2022; Zhu & Quiring, 2022).

437
438 Moreover, the choice of observation dataset is a key factor for assessing the impact of the
439 horizontal resolution and model time step on extreme precipitation. Most observation
440 precipitation data are from one of the three categories, gauge-based products, satellite products,
441 and merged satellite-gauge products. Since the satellite products are constructed with satellite
442 microwave and/ or infrared measurements, with/ without gauged-adjusted estimates,
443 differences exist between these products. Besides, the gauge-based products are highly
444 dependent on the choice of stations and interpolation schemes. It is hard to say which product
445 is closer to reality, as different regions may have different observation datasets that suit best
446 for the analysis. In particular, we note that not all products are suitable for extreme analysis.
447 For example, GPCP's main scope is to construct a reliable climate data record and has been
448 developed with a priority of ensuring the long-term stability of data (Adler et al., 2017).
449 Masunaga et al. (2019) found that the frequency of GPCP daily precipitation quickly drops
450 below all other datasets once the precipitation exceeds 30 mm/d. Also, the time series of GPCP
451 extreme precipitation over the ocean exhibits a jump to lower 99th percentiles in late 2008/early
452 2009 which is not present in all other datasets, coinciding with the change in utilization of
453 SSM/I and SSMIS. The lower 99th precipitation suggests that the GPCP dataset might not be
454 applied to extreme analysis (Masunaga et al., 2019). Therefore, we only use GPCP observation
455 data as the reference to explore the model performance. In Fig. 2f–i the 99th percentile
456 precipitation is largely underestimated in the eastern Alp region by ERA5 and all model
457 simulations. The biases are insensitive to horizontal resolution. It is likely a persistent model
458 bias in the ECMWF-IFS or a bias in GPCP. Analyzing multiple precipitation products instead
459 of relying on a single one may be a good way to reduce these biases.

460

461 **Code and data variability**

462 The OpenIFS model requires a software license agreement with ECMWF to use it, and
463 OpenIFS's license is easily given free of charge to any academic or research institute. The
464 details of OpenIFS are available at
465 <https://confluence.ecmwf.int/display/OIFS/About+OpenIFS> (ECMWF, 2018). We used the
466 same simulation that used in Savita et al. (2024) and therefore do not provide the data needed



467 to reproduce the simulations here. All data (runscripts, input data etc) needed to reproduce the
468 simulations can be found in Savita et al. (2024) in code and data variability section. The jupyter
469 notebook scripts used in this study to produce the plots can be found at
470 <https://doi.org/10.5281/zenodo.10887652>. The raw model output is available from the authors
471 upon reasonable request. The observation and reanalysis datasets used in this study can be
472 downloaded from GPCC ([https://opendata.dwd.de/climate_environment/GPCC/html/fulldata-](https://opendata.dwd.de/climate_environment/GPCC/html/fulldata-daily_v2022_doi_download.html)
473 [daily_v2022_doi_download.html](https://opendata.dwd.de/climate_environment/GPCC/html/fulldata-daily_v2022_doi_download.html), Ziese et al., 2022) and ERA5
474 (<https://cds.climate.copernicus.eu/cdsapp#!/dataset/reanalysis-era5-single-levels?tab=form>,
475 Hersbach et al., 2023).

476

477 **Authors contributions.** AS and JK conducted all the OpenIFS simulations. YL did the
478 analysis and writing with substantial contribution from JK, AS and WP.

479

480 **Competing interests.** The contact author has declared that none of the authors has any
481 competing interests.

482

483 **Acknowledgements.** Yingxue Liu is supported by China Scholarship Council (CSC, grant no.
484 202004910401). Joakim Kjellsson and Abhishek Savita are supported by JPI Climate/Ocean
485 (ROADMAP project, grant no. 01LP2002C). Wonsun Park was supported by IBS (grant no.
486 IBS-R028-D1). We thank the OpenIFS team at ECMWF for the technical support. All the
487 OpenIFS simulations were conducted on the HLRN machine under shk00018 project resources.
488 All the analysis and data storage were conducted on computer clusters at GEOMAR and Kiel
489 University Computing Center (NESH).

490

491 **Financial support.** This research is financially supported by CSC (grant no. 202004910401)
492 and ROADMAP project (grant no. 01LP2002C).

493

494

495

496

497

498

499

500



501 References

- 502 Adler, R. F., Gu, G., Sapiano, M., Wang, J. J., & Huffman, G. J. (2017). Global
503 Precipitation: Means, Variations and Trends During the Satellite Era (1979–2014).
504 In *Surveys in Geophysics* (Vol. 38, Issue 4, pp. 679–699). Springer Netherlands.
505 <https://doi.org/10.1007/s10712-017-9416-4>
- 506 Alexander, L. V., Fowler, H. J., Bador, M., Behrangi, A., Donat, M. G., Dunn, R., Funk,
507 C., Goldie, J., Lewis, E., Rogé, M., Seneviratne, S. I., & Venugopal, V. (2019). On
508 the use of indices to study extreme precipitation on sub-daily and daily timescales.
509 *Environmental Research Letters*, 14(12). <https://doi.org/10.1088/1748-9326/ab51b6>
- 510 Avila, F. B., Dong, S., Menang, K. P., Rajczak, J., Renom, M., Donat, M. G., &
511 Alexander, L. V. (2015). Systematic investigation of gridding-related scaling
512 effects on annual statistics of daily temperature and precipitation maxima: A case
513 study for south-east Australia. *Weather and Climate Extremes*, 9, 6–16.
514 <https://doi.org/10.1016/j.wace.2015.06.003>
- 515 Bacmeister, J. T., Wehner, M. F., Neale, R. B., Gettelman, A., Hannay, C., Lauritzen, P.
516 H., Caron, J. M., & Truesdale, J. E. (2014). Exploratory high-resolution climate
517 simulations using the community atmosphere model (CAM). *Journal of Climate*,
518 27(9), 3073–3099. <https://doi.org/10.1175/JCLI-D-13-00387.1>
- 519 Bador, M., Boé, J., Terray, L., Alexander, L. V., Baker, A., Bellucci, A., Haarsma, R.,
520 Koenigk, T., Moine, M. P., Lohmann, K., Putrasahan, D. A., Roberts, C., Roberts,
521 M., Scoccimarro, E., Schiemann, R., Seddon, J., Senan, R., Valcke, S., & Vanniere,
522 B. (2020). Impact of Higher Spatial Atmospheric Resolution on Precipitation
523 Extremes Over Land in Global Climate Models. *Journal of Geophysical Research:*
524 *Atmospheres*, 125(13). <https://doi.org/10.1029/2019JD032184>
- 525 Barrett, A. I., Wellmann, C., Seifert, A., Hoose, C., Vogel, B., & Kunz, M. (2019). One
526 Step at a Time: How Model Time Step Significantly Affects Convection-Permitting
527 Simulations. *Journal of Advances in Modeling Earth Systems*, 11(3), 641–658.
528 <https://doi.org/10.1029/2018MS001418>
- 529 Bell, B., Hersbach, H., Simmons, A., Berrisford, P., Dahlgren, P., Horányi, A., Muñoz-
530 Sabater, J., Nicolas, J., Radu, R., Schepers, D., Soci, C., Villaume, S., Bidlot, J. R.,
531 Haimberger, L., Woollen, J., Buontempo, C., & Thépaut, J. N. (2021). The ERA5
532 global reanalysis: Preliminary extension to 1950. *Quarterly Journal of the Royal*
533 *Meteorological Society*, 147(741), 4186–4227. <https://doi.org/10.1002/qj.4174>
- 534 Caldwell, P. (2010). California wintertime precipitation bias in regional and global
535 climate models. *Journal of Applied Meteorology and Climatology*, 49(10), 2147–
536 2158. <https://doi.org/10.1175/2010JAMC2388.1>
- 537 Cariolle, D., & Teyssède, H. (2007). Atmospheric Chemistry and Physics A revised
538 linear ozone photochemistry parameterization for use in transport and general
539 circulation models: multi-annual simulations. In *Atmos. Chem. Phys* (Vol. 7).
540 www.atmos-chem-phys.net/7/2183/2007/
- 541 Chan, S. C., Kendon, E. J., Fowler, H. J., Blenkinsop, S., Ferro, C. A. T., & Stephenson,
542 D. B. (2013). Does increasing the spatial resolution of a regional climate model
543 improve the simulated daily precipitation? *Climate Dynamics*, 41(5–6), 1475–1495.
544 <https://doi.org/10.1007/s00382-012-1568-9>
- 545 Delworth, T. L., Rosati, A., Anderson, W., Adcroft, A. J., Balaji, V., Benson, R., Dixon,
546 K., Griffies, S. M., Lee, H. C., Pacanowski, R. C., Vecchi, G. A., Wittenberg, A.
547 T., Zeng, F., & Zhang, R. (2012). Simulated climate and climate change in the
548 GFDL CM2.5 high-resolution coupled climate model. *Journal of Climate*, 25(8),
549 2755–2781. <https://doi.org/10.1175/JCLI-D-11-00316.1>



- 550 Demory, M. E., Berthou, S., Fernández, J., Sørland, S. L., Brogli, R., Roberts, M. J.,
551 Beyerle, U., Seddon, J., Haarsma, R., Schär, C., Buonomo, E., Christensen, O. B.,
552 Ciarlo, J. M., Fealy, R., Nikulin, G., Peano, D., Putrasahan, D., Roberts, C. D.,
553 Senan, R., ... Vautard, R. (2020). European daily precipitation according to EURO-
554 CORDEX regional climate models (RCMs) and high-resolution global climate
555 models (GCMs) from the High-Resolution Model Intercomparison Project
556 (HighResMIP). *Geoscientific Model Development*, 13(11), 5485–5506.
557 <https://doi.org/10.5194/gmd-13-5485-2020>
- 558 Gori, A., Lin, N., Xi, D., & Emanuel, K. (2022). Tropical cyclone climatology change
559 greatly exacerbates US extreme rainfall–surge hazard. *Nature Climate Change*,
560 12(2), 171–178. <https://doi.org/10.1038/s41558-021-01272-7>
- 561 Graham, R. M., Hudson, S. R., & Maturilli, M. (2019). Improved Performance of ERA5
562 in Arctic Gateway Relative to Four Global Atmospheric Reanalyses. *Geophysical
563 Research Letters*, 46(11), 6138–6147. <https://doi.org/10.1029/2019GL082781>
- 564 Hassler, B., & Lauer, A. (2021). Comparison of reanalysis and observational
565 precipitation datasets including era5 and wfde5. *Atmosphere*, 12(11).
566 <https://doi.org/10.3390/atmos12111462>
- 567 Hersbach, H., Bell, B., Berrisford, P., Hirahara, S., Horányi, A., Muñoz-Sabater, J.,
568 Nicolas, J., Peubey, C., Radu, R., Schepers, D., Simmons, A., Soci, C., Abdalla, S.,
569 Abellan, X., Balsamo, G., Bechtold, P., Biavati, G., Bidlot, J., Bonavita, M., ...
570 Thépaut, J. N. (2020). The ERA5 global reanalysis. *Quarterly Journal of the Royal
571 Meteorological Society*, 146(730), 1999–2049. <https://doi.org/10.1002/qj.3803>
- 572 Hertwig, E., von Storch, J. S., Handorf, D., Dethloff, K., Fast, I., & Krismer, T. (2015).
573 Effect of horizontal resolution on ECHAM6-AMIP performance. *Climate
574 Dynamics*, 45(1–2), 185–211. <https://doi.org/10.1007/s00382-014-2396-x>
- 575 Hyndman, R. J., & Fan, Y. (1996). Sample Quantiles in Statistical Packages. In *Source:
576 The American Statistician* (Vol. 50, Issue 4).
- 577 Iles, C. E., Vautard, R., Strachan, J., Joussaume, S., Eggen, B. R., & Hewitt, C. D.
578 (2020). The benefits of increasing resolution in global and regional climate
579 simulations for European climate extremes. *Geoscientific Model Development*,
580 13(11), 5583–5607. <https://doi.org/10.5194/gmd-13-5583-2020>
- 581 Intergovernmental Panel on Climate Change. (2023). Weather and Climate Extreme
582 Events in a Changing Climate. In *Climate Change 2021 – The Physical Science
583 Basis* (pp. 1513–1766). Cambridge University Press.
584 <https://doi.org/10.1017/9781009157896.013>
- 585 Jones, P. W. (1998). *First-and Second-Order Conservative Remapping Schemes for
586 Grids in Spherical Coordinates*.
- 587 Jong, B. T., Delworth, T. L., Cooke, W. F., Tseng, K. C., & Murakami, H. (2023).
588 Increases in extreme precipitation over the Northeast United States using high-
589 resolution climate model simulations. *Npj Climate and Atmospheric Science*, 6(1).
590 <https://doi.org/10.1038/s41612-023-00347-w>
- 591 Jung, T., Miller, M. J., Palmer, T. N., Towers, P., Wedi, N., Achuthavarier, D., Adams,
592 J. M., Altshuler, E. L., Cash, B. A., Kinter, J. L., Marx, L., Stan, C., & Hodges, K.
593 I. (2012). High-resolution global climate simulations with the ECMWF model in
594 project athena: Experimental design, model climate, and seasonal forecast skill.
595 *Journal of Climate*, 25(9), 3155–3172. <https://doi.org/10.1175/JCLI-D-11-00265.1>
- 596 Khairoutdinov, M., & Kogan, Y. (2000). *A New Cloud Physics Parameterization in a
597 Large-Eddy Simulation Model of Marine Stratocumulus*.



- 598 Kopparla, P., Fischer, E. M., Hannay, C., & Knutti, R. (2013). Improved simulation of
599 extreme precipitation in a high-resolution atmosphere model. *Geophysical*
600 *Research Letters*, *40*(21), 5803–5808. <https://doi.org/10.1002/2013GL057866>
601 Laprise, R. (2008). Regional climate modelling. *Journal of Computational Physics*,
602 *227*(7), 3641–3666. <https://doi.org/10.1016/j.jcp.2006.10.024>
603 Lavers, D. A., Simmons, A., Vamborg, F., & Rodwell, M. J. (2022). An evaluation of
604 ERA5 precipitation for climate monitoring. *Quarterly Journal of the Royal*
605 *Meteorological Society*, *148*(748), 3152–3165. <https://doi.org/10.1002/qj.4351>
606 Li, C., Zwiers, F., Zhang, X., Li, G., Sun, Y., & Wehner, M. (2021). Changes in Annual
607 Extremes of Daily Temperature and Precipitation in CMIP6 Models. *Journal of*
608 *Climate*, *34*, 3441–3460. <https://doi.org/10.1175/JCLI-D-19>
609 Malardel, S., Wedi, N., Deconinck, W., & Kühnlein, C. (2016). *A new grid for the IFS*.
610 <https://www.researchgate.net/publication/297695132>
611 Masunaga, H., Schröder, M., Furuzawa, F. A., Kummerow, C., Rustemeier, E., &
612 Schneider, U. (2019). Inter-product biases in global precipitation extremes.
613 *Environmental Research Letters*, *14*(12). <https://doi.org/10.1088/1748-9326/ab5da9>
614 Mishra, S. K., & Sahany, S. (2011). Effects of time step size on the simulation of
615 tropical climate in NCAR-CAM3. *Climate Dynamics*, *37*(3), 689–704.
616 <https://doi.org/10.1007/s00382-011-0994-4>
617 Monerie, P. A., Chevuturi, A., Cook, P., Klingaman, N. P., & Holloway, C. E. (2020).
618 Role of atmospheric horizontal resolution in simulating tropical and subtropical
619 South American precipitation in HadGEM3-GC31. *Geoscientific Model*
620 *Development*, *13*(10), 4749–4771. <https://doi.org/10.5194/gmd-13-4749-2020>
621 Myhre, G., Alterskjær, K., Stjern, C. W., Hodnebrog, M., Marelle, L., Samset, B. H.,
622 Sillmann, J., Schaller, N., Fischer, E., Schulz, M., & Stohl, A. (2019). Frequency of
623 extreme precipitation increases extensively with event rareness under global
624 warming. *Scientific Reports*, *9*(1). <https://doi.org/10.1038/s41598-019-52277-4>
625 O’Gorman, P. A. (2015). Precipitation Extremes Under Climate Change. In *Current*
626 *Climate Change Reports* (Vol. 1, Issue 2, pp. 49–59). Springer.
627 <https://doi.org/10.1007/s40641-015-0009-3>
628 Prein, A. F., Gobiet, A., Suklitsch, M., Truhetz, H., Awan, N. K., Keuler, K., &
629 Georgievski, G. (2013). Added value of convection permitting seasonal
630 simulations. *Climate Dynamics*, *41*(9–10), 2655–2677.
631 <https://doi.org/10.1007/s00382-013-1744-6>
632 Rauscher, S. A., O’Brien, T. A., Piani, C., Coppola, E., Giorgi, F., Collins, W. D., &
633 Lawston, P. M. (2016). A multimodel intercomparison of resolution effects on
634 precipitation: simulations and theory. *Climate Dynamics*, *47*(7–8), 2205–2218.
635 <https://doi.org/10.1007/s00382-015-2959-5>
636 Savita, A., Kjellsson, J., Kedzierski, R. P., Latif, M., Rahm, T., Wahl, S., & Park, W.
637 (2024). Assessment of climate biases in OpenIFS version 43r3 across model
638 horizontal resolutions and time steps. *Geoscientific Model Development*, *17*(4),
639 1813–1829. <https://doi.org/10.5194/gmd-17-1813-2024>
640 Schiemann, R., Demory, M. E., Mizielinski, M. S., Roberts, M. J., Shaffrey, L. C.,
641 Strachan, J., & Vidale, P. L. (2014). The sensitivity of the tropical circulation and
642 Maritime Continent precipitation to climate model resolution. *Climate Dynamics*,
643 *42*(9–10), 2455–2468. <https://doi.org/10.1007/s00382-013-1997-0>
644 Sillmann, J., Kharin, V. V., Zhang, X., Zwiers, F. W., & Bronaugh, D. (2013). Climate
645 extremes indices in the CMIP5 multimodel ensemble: Part I. Model evaluation in
646 the present climate. *Journal of Geophysical Research Atmospheres*, *118*(4), 1716–
647 1733. <https://doi.org/10.1002/jgrd.50203>



- 648 Strandberg, G., & Lind, P. (2021). The importance of horizontal model resolution on
649 simulated precipitation in Europe – from global to regional models. *Weather and*
650 *Climate Dynamics*, 2(1), 181–204. <https://doi.org/10.5194/wcd-2-181-2021>
651 Sundqvist, H. (1978). A parameterization scheme for non-convective condensation
652 including prediction of cloud water content. *Quarterly Journal of the Royal*
653 *Meteorological Society*, 104(441), 677–690.
654 <https://doi.org/10.1002/qj.49710444110>
655 Tarek, M., Brissette, F. P., & Arsenault, R. (2020). Evaluation of the ERA5 reanalysis as
656 a potential reference dataset for hydrological modelling over North America.
657 *Hydrology and Earth System Sciences*, 24(5), 2527–2544.
658 <https://doi.org/10.5194/hess-24-2527-2020>
659 Tetzner, D., Thomas, E., & Allen, C. (2019). A validation of ERA5 reanalysis data in
660 the southern antarctic peninsula—Ellsworth land region, and its implications for ice
661 core studies. *Geosciences (Switzerland)*, 9(7).
662 <https://doi.org/10.3390/geosciences9070289>
663 Torma, C., Giorgi, F., & Coppola, E. (2015). Added value of regional climate modeling
664 over areas characterized by complex terrain-precipitation over the Alps. *Journal of*
665 *Geophysical Research*, 120(9), 3957–3972. <https://doi.org/10.1002/2014JD022781>
666 Wan, H., Zhang, S., Rasch, P. J., Larson, V. E., Zeng, X., & Yan, H. (2021).
667 Quantifying and attributing time step sensitivities in present-day climate
668 simulations conducted with EAMv1. *Geoscientific Model Development*, 14(4),
669 1921–1948. <https://doi.org/10.5194/gmd-14-1921-2021>
670 Wang, C., Graham, R. M., Wang, K., Gerland, S., & Granskog, M. A. (2019).
671 Comparison of ERA5 and ERA-Interim near-surface air temperature, snowfall and
672 precipitation over Arctic sea ice: effects on sea ice thermodynamics and evolution.
673 *Cryosphere*, 13(6), 1661–1679. <https://doi.org/10.5194/tc-13-1661-2019>
674 Wehner, M. F., Reed, K. A., Li, F., Prabhat, Bacmeister, J., Chen, C. T., Paciorek, C.,
675 Gleckler, P. J., Sperber, K. R., Collins, W. D., Gettelman, A., & Jablonowski, C.
676 (2014). The effect of horizontal resolution on simulation quality in the Community
677 Atmospheric Model, CAM5.1. *Journal of Advances in Modeling Earth Systems*,
678 6(4), 980–997. <https://doi.org/10.1002/2013MS000276>
679 Wehner, M. F., Smith, R. L., Bala, G., & Duffy, P. (2010). The effect of horizontal
680 resolution on simulation of very extreme US precipitation events in a global
681 atmosphere model. *Climate Dynamics*, 34(2), 241–247.
682 <https://doi.org/10.1007/s00382-009-0656-y>
683 Xu, X., Frey, S. K., Boluwade, A., Erler, A. R., Khader, O., Lapen, D. R., & Sudicky, E.
684 (2019). Evaluation of variability among different precipitation products in the
685 Northern Great Plains. *Journal of Hydrology: Regional Studies*, 24.
686 <https://doi.org/10.1016/j.ejrh.2019.100608>
687 Zhu, L., & Quiring, S. M. (2022). Exposure to precipitation from tropical cyclones has
688 increased over the continental United States from 1948 to 2019. *Communications*
689 *Earth and Environment*, 3(1). <https://doi.org/10.1038/s43247-022-00639-8>
690

691

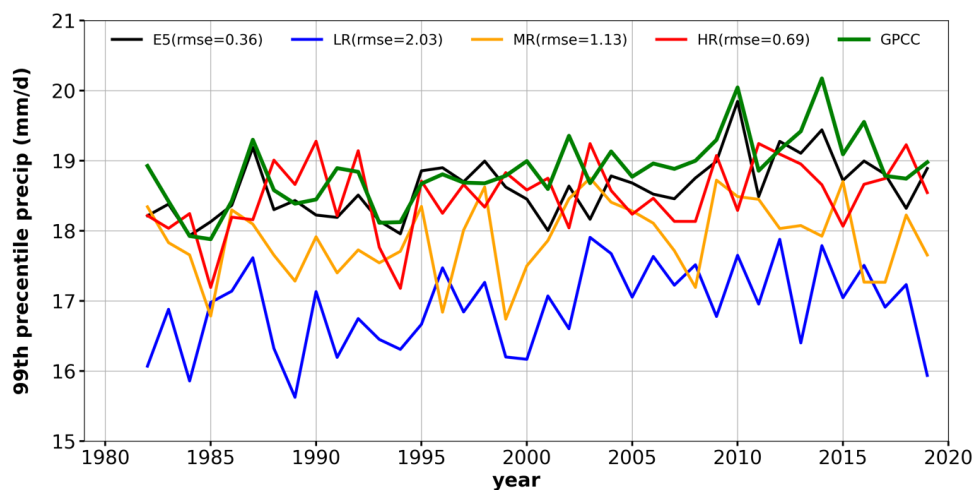
692

693



694

Figures



695
696

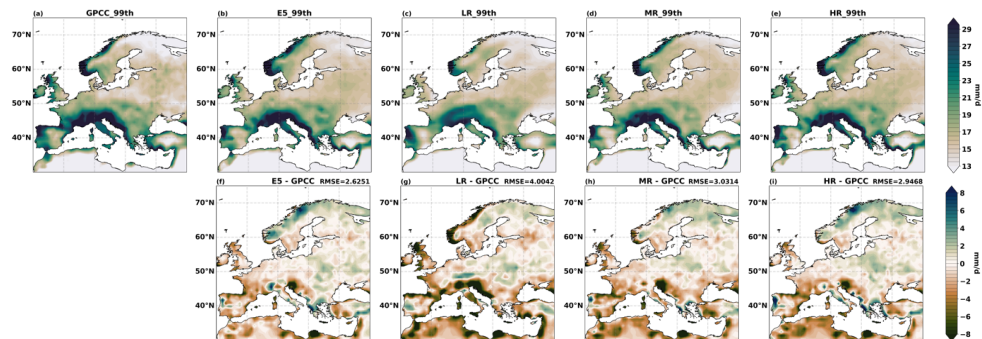
697 **Fig. 1** Annual time series of the 99th percentile precipitation using observations (GPCC, green),
698 reanalysis (ERA5, black), and model simulations (LR: blue, MR: orange, HR: red) during
699 1982-2019 over Europe. RMSE values of 99th percentile precipitation are computed referenced
700 to GPCC which are shown within the small bracket.

701
702
703
704
705
706
707
708
709
710
711
712
713
714
715
716
717
718
719
720
721
722
723
724



725

726



727

728

729

730

731

732

733

734

735

736

737

738

739

740

741

742

743

744

745

746

747

748

749

750

751

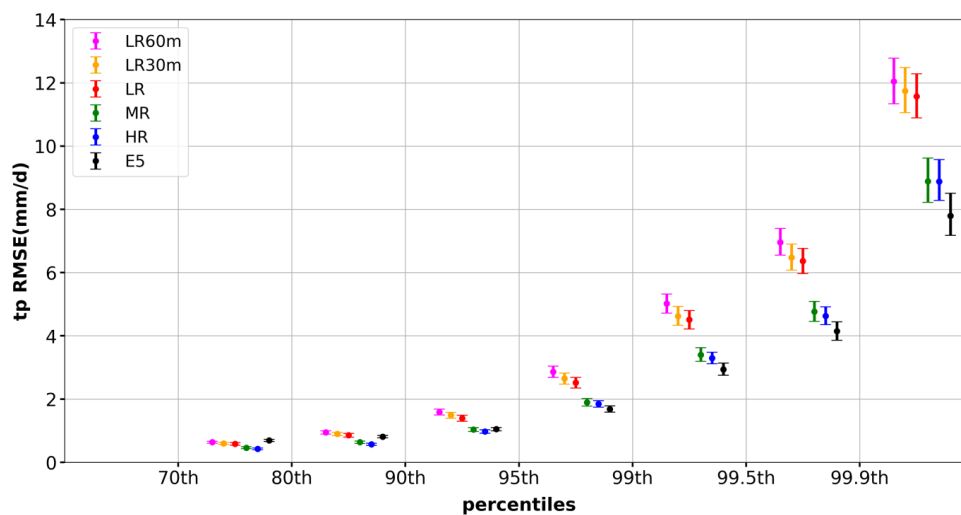
752

753

754

755

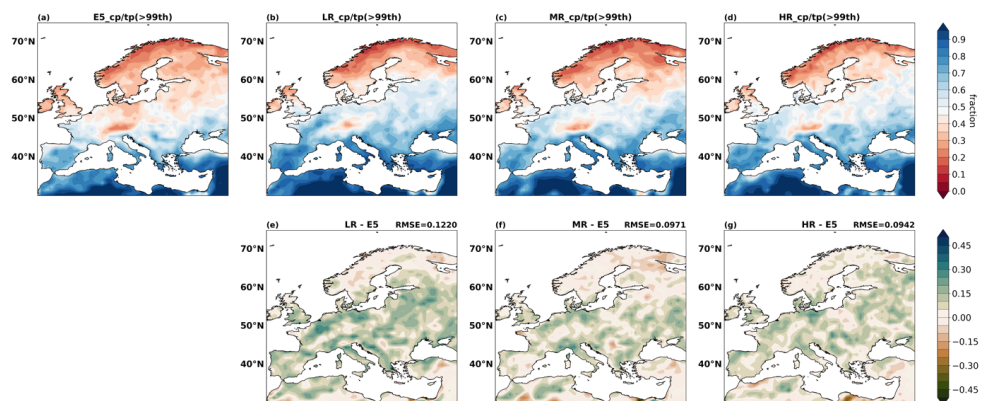
Fig. 2 The 99th percentile precipitation over Europe during 1982-2019 from (a) GPCC observations, (b) ERA5 reanalysis, (c) LR, (d) MR, (e) HR, and the corresponding biases and RMSEs in (f) ERA5, (g) LR, (h) MR, and (i) HR.



756
757

758 **Fig. 3** RMSEs for annual total precipitation at different percentile ranges (70th – 80th –
759 90th, 80th – 90th, 90th – 95th, 95th – 99th, 99th – 99.5th, 99.5th – 99.9th and >99.9th percentile) in ERA5 (black)
760 and OpenIFS simulations (LR60m: magenta, LR30m: orange, LR: red, MR: green, HR: blue)
761 referenced to GPCC during 1982-2019 over Europe. Dots are the RMSE values, and error bars
762 are the 95 % CI.

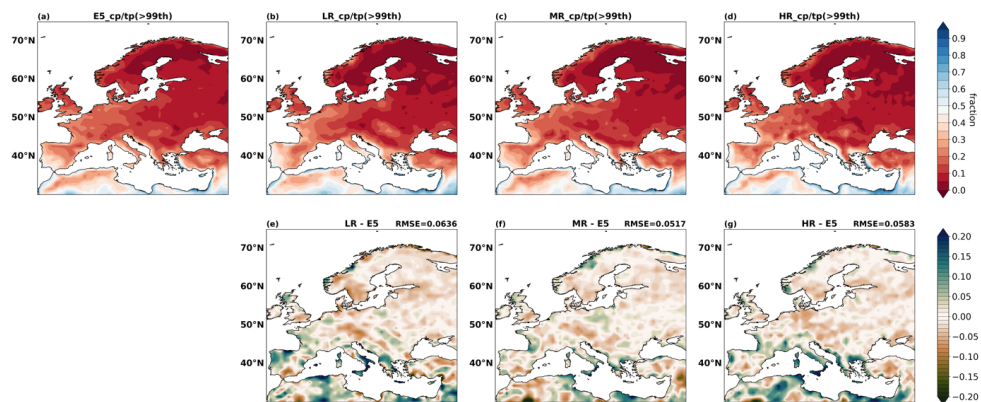
763
764
765
766
767
768
769
770
771
772
773
774
775
776
777
778
779



780
781

782 **Fig. 4** Contribution of convective precipitation to extreme precipitation (>99th percentile) in (a)
783 ERA5, (b) LR, (c) MR and (d) HR over Europe in JJA, and (e)– (g) their biases and RMSEs
784 compared to ERA5 over the period 1982-2019.

785



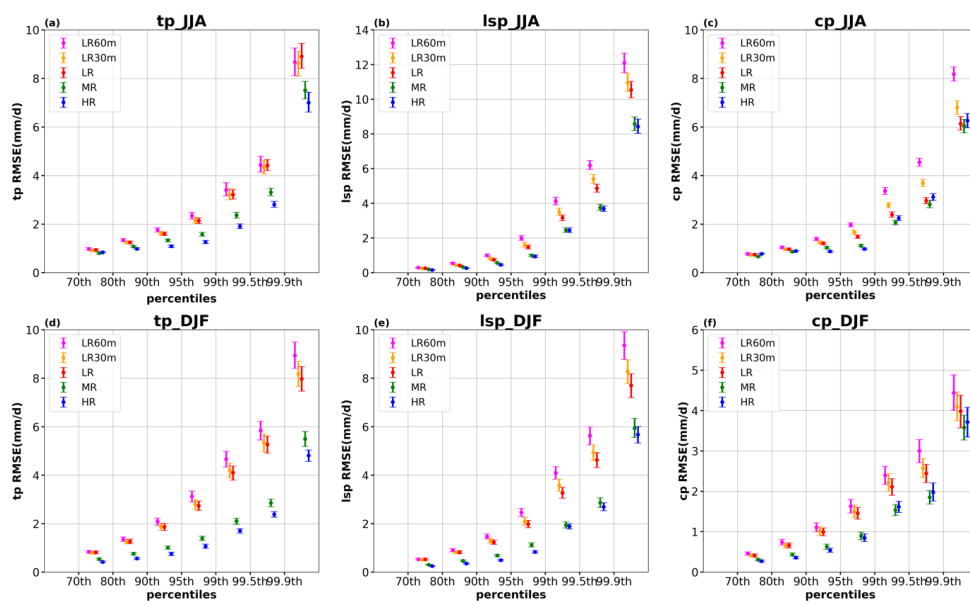
786
787

788 **Fig. 5** The same as Fig. 4 but for DJF.

789
790
791
792
793
794
795
796
797



798



799
800

801 **Fig. 6** RMSEs of total precipitation (a & d) at different percentile ranges (70th – 80th –
802 90th, 90th – 95th, 95th – 99th, 99th – 99.5th, 99.5th – 99.9th and >99.9th) and the corresponding
803 large-scale precipitation (b & e) and convective precipitation (c & f) in OpenIFS simulations
804 (LR60m: magenta, LR30m: orange, LR: red, MR: green, HR: blue) against ERA5 over Europe
805 during 1982-2019. (a) – (c) are for JJA, and (d) – (f) for DJF. Dots are the RMSE values, and
806 error bars are the 95 % confidence intervals. Unit is mm/d.

807

808

809

810

811

812

813

814

815

816

817

818

819

820

821

822

823



824
825

Table

826 Table 1: The experiment details of different horizontal resolutions and model time steps in
827 OpenIFS.

	LR60m	LR30m	LR	MR	HR
Vertical resolution	L91			L91	L91
Horizontal Resolution	100 km (Tco95)			50 km (Tco199)	25 km (Tco399)
Time steps	60 minutes	30 minutes	15 minutes	15 minutes	15 minutes

828